JOURNAL OF MATERIALS SCIENCE 28 (1993) 1946–1956

Phase transformations and structure–property relationships in a rapidly solidified Ni–Al–Mo alloy

Part I *Phase transformations*

SANG YUL LEE*, P. NASH
Illinois Institute of Technology, Chicago, IL 60616, USA

An Ni–Al–Mo–V–Re alloy was melt-spun at 30 $m s^{-1}$ to produce a completely solutionized metastable solid solution. The phase transformation sequences on subsequent ageing of this material over a range of temperatures from 650 to 800 °C were studied using transmission electron microscopy. The results showed that the transformation behaviour was independent of the ageing temperature over the range studied, but with increased transformation kinetics on increasing the temperature. A complex transformation sequence was found involving spinodal ordering, precipitation of metastable phases and discontinuous transformation. In addition, while equilibrium Ni_3Mo phase was involved in the transformation sequence, the δ (NiMo) phase was not observed for the heat treatment range studied. The results of the phase transformation sequence of this alloy are correlated with the corresponding physical and mechanical properties of the material in Part II.

1. Introduction

The phase transformations in Ni-rich Ni–Mo binary alloys have been studied extensively and very complex ordering sequences depending upon alloy composition and ageing temperature have been reported [1–7]. It is not surprising, therefore, to observe similar complex phase transformation behaviour in ternary and higher-order Ni–Mo-based alloys [8–10]. The effects of alloying on the phase transformations of Ni–Mo-based alloys have been reviewed elsewhere [11] and the effects of alloying on the metastable phase stability have been studied by several investigators [4–6, 10], the results were interpreted in terms of either the change in the ratio of the second to first nearest-neighbour pair interaction potential, V_2/V_1, or a substitutional size effect. For example, addition of Al [6] or V [7] were reported to stabilize the metastable $Ni_3Mo(D0_{22})$ phase while destabilizing the metastable Ni_2Mo phase. Based on the statistical thermodynamic theory developed by Clapp and Moss [12–14] and extended by de Fontaine [15, 16], the coherent phase diagram of the Ni–Mo system for three V_2/V_1 ratios showed an increase in the stability of the metastable Ni_3Mo phase, confirming the conclusion based on experiments [5, 6].

The objectives of this work were to study the phase transformations in Ni–Al–Mo alloy resulting from isothermal ageing. Particular attention was paid to the evolution of the embrittling δ (NiMo) phase on ageing below 1000 °C and to the stabilities of the metastable phases. The corresponding variation of physical and mechanical properties of this alloy on isothermal ageing are presented in Part II [17].

2. Experimental procedure

The method of sample preparation has been described in a previous paper [18]. An alloy with a composition of Ni–13.5 at % Al–19.2 at % Mo–1.9 at % V–0.4 at % Re was melt-spun at 30 $m s^{-1}$ using a chilled block melt-spinning (CBMS) process to produce a continuous ribbon.

The ribbons were encapsulated in a quartz tube under an Ar atmosphere of 1.33 kPa and were heat-treated at four different temperatures and a series of times. Samples to be aged for less than 4 min were not sealed in a quartz tube, but were put into a tantalum boat and aged in air. Although some surface oxidation occurred this was done in order to ensure accuracy of the heat treatment time. Discs, 3 mm in diameter, were electropolished using a double-jet Tenupol polisher with a solution of 10% perchloric acid in methanol kept at − 60 °C during the electropolishing process.

Since the microstructural features of aged specimens are very complex due to the presence of multiple phases, coherency strains and double diffraction, dark-field images (DFI) and selected-area diffraction patterns (SADP) were incorporated with bright-field images (BFI) to identify the phases. For SADP, long photographic exposures of up to 3 min with a defocused second condenser lens were used to record the very weak diffraction spots. Despite the complexity of

Present address: KIMM, 66 Sangnam-Dong, Changwan, Kyungnam, South Korea.

0022–2461

the ageing sequence, SADP analysis is adequate for identification of phases which are well established in the literature. Transmission electron microscopy (TEM) samples were examined in a JEOL 100 CX at 100 kV and a Phillips 400EM at 120 kV.

3. Results and discussion

Rapid solidification of this alloy using the CBMS process with a wheel speed of 30 m s^{-1} resulted in complete solutionization of the alloying elements as reported previously [18]. Therefore this as-cast ribbon was used as starting material to study the microstructural development as a function of ageing time at different ageing temperatures from 650° to 800 °C.

Very complex transformation behaviours were observed in this alloy. Knowing the complex ordering transformations of the binary Ni–Mo alloys [3, 7, 19–23] even more complex transformations were expected in this alloy. The transformation sequences studied in this work at different temperatures were very similar, except that the transformation kinetics increased as ageing temperature increased. In the following discussion the aged specimens will be referred to by their heat treatment time in minutes and temperature, e.g. 1/650 indicates ageing for 1 min at 650 °C.

For specimen 1/650, the microstructure (Fig. 1) was similar to that of as-cast ribbon, showing a modulated structure within the cells. However, the inset SADP in Fig. 1 exhibited weak $\gamma'(Ni_3Al)$ superlattice spots, satellite spots in $\langle 1\,0\,0 \rangle$ around the fundamental reflections, and very weak streaks running through the fundamental reflections in $\langle 1\,0\,0 \rangle$. Also, the diffuse intensity around the fundamental spots observed in the as-cast ribbon was still present. On further ageing at 650 °C the diffuse intensity around the fundamental reflections decreased as compared with that of as-cast ribbons and became more confined to form $\langle 1\,0\,0 \rangle$ streaks as shown in Fig. 2. At the same time the intensity of the $\gamma'(Ni_3Al)$ spots as well as that of the satellite spots around the fundamentals increased. In other words, continuous transfer of diffuse intensity around the fundamental spots toward the superlattice spots occurred as ageing proceeded. This diffraction evidence suggests that the early-stage decomposition of the supersaturated disordered f.c.c. γ(Ni) solution with short range-order occurs by means of spinodal ordering (or continuous ordering), as defined by de Fontaine [15]. An ordering transformation by a spinodal ordering mechanism has been reported in Ni–Mo-based alloys [6, 10, 20, 23] as well as in many other alloy systems, such as Ni–Ti, Cu-base alloys and Co-base alloys [1].

By measuring the Δg (length of the displacement vector from the diffraction spot to the satellite spot) from SADP the composition modulation wavelength during spinodal ordering was determined using the Daniel–Lipson equation [24]:

$$\lambda = \frac{ah}{h^2 + k^2 + l^2}\left(\frac{g}{\Delta g}\right)$$

where λ = modulation wavelength, a = lattice parameter, $h\ k\ l$ = Miller indices and g = length of the reciprocal lattice vector of the plane used. The lattice parameter of the supersaturated solid solution of this alloy (a_γ) was measured to be 0.3646 nm [25]. The results of the composition modulation wavelength as a function of ageing time and temperature are summarized in Fig. 3, which shows that the cube of the

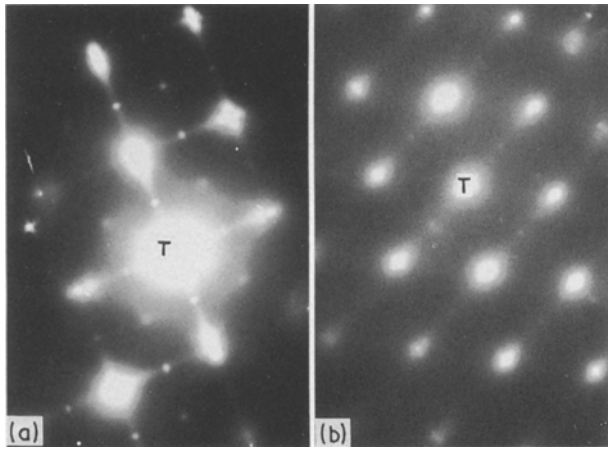

Figure 2 Selected-area diffraction patterns of ribbon after ageing for 5 min at 650 °C: (a) [0 0 1] zone, (b) [0 1 1] zone.

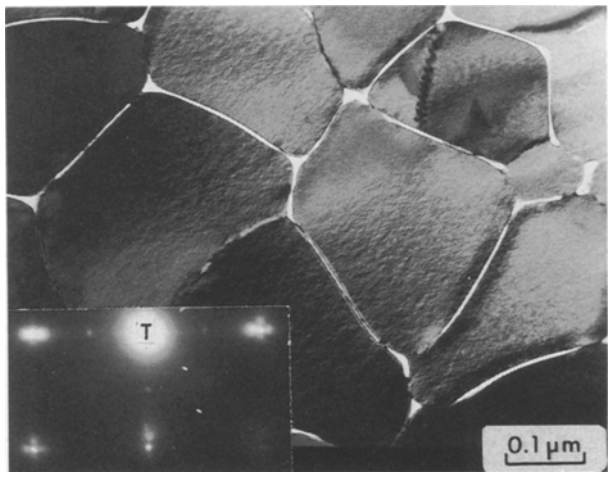

Figure 1 TEM micrographs of ribbon after ageing for 1 min at 650 °C. [0 0 1] zone for the inset diffraction pattern.

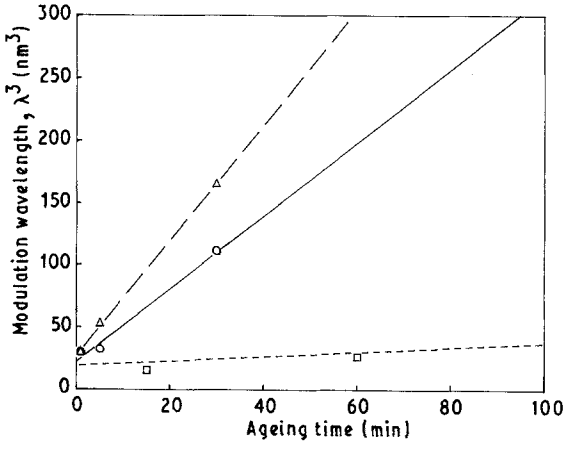

Figure 3 Modulation wavelengths as a function of ageing time and temperature: (□) 600 °C, (○) 650 °C, (△) 700 °C.

wavelength is linearly proportional to the ageing time in the early stage, implying that spinodal ordering is controlled by a volume diffusion process.

The microstructural features of specimen 30/650 (Fig. 4) were very similar to those of 5/700. The BFI in Fig. 4 shows a coarsened modulated structure in the cells, giving rise to a smaller Δg. Precipitates (as indicated by the arrow) were observed at the cell boundaries in dark-field imaging, using a diffracted spot indicated by an arrow in the inset SADP. These precipitates were identified to be α(Mo) phase. The inset SADP exhibits strong and sharp streaking in ⟨1 0 0⟩ and reflections from the α(Mo) precipitates as indicated by the arrow. Being very strong and sharp the ⟨0 0 1⟩ streaks from the fundamental spots did not seem to be solely due to spinodal ordering. In fact, close examination of the inset SADP also revealed streaking of $\gamma'(Ni_3Al)$ superlattice spots in ⟨1 0 0⟩. Since $\gamma'(Ni_3Al)$ precipitates generally have a cuboidal form, aligned in ⟨1 0 0⟩ with $(1\,0\,0)_\gamma \| (100)_{\gamma'}$ a strong streaking in ⟨1 0 0⟩ due to fine cubic particles is expected. Therefore the ⟨1 0 0⟩ streaking is partly due to a diffraction effect caused by precipitate shape [26]. The SADP with ⟨0 1 1⟩ zone axis also exhibits streaking in ⟨1 0 0⟩. However, it is also possible that the streaking in ⟨1 0 0⟩ might be due to elastic strain in the ⟨1 0 0⟩ direction associated with the modulated structure produced by spinodal ordering (note that the elastically soft direction in Ni-base f.c.c. material is ⟨1 0 0⟩). The coarsened modulated structure in the cell implies the formation of discrete $\gamma'(Ni_3Al)$ precipitates, even though they are still too fine to be resolved. Therefore the ⟨1 0 0⟩ streaking in Fig. 4 could be due to a combination of spinodal ordering, shape effect, and elastic strain. It was difficult to identify the exact cause for streaking using conventional TEM. Even though it was much reduced, the diffuse intensity around the fundamental reflections was still present in 30/650, suggesting that spinodal ordering was still in progress.

Fig. 5 shows the microstructure of specimen 45/700. Thin plate-like precipitates were observed in the cells with sizes of the order of 40 nm in length and 3 nm in width. These plate-like precipitates were nucleated homogeneously in the cells and were identified to be α(Mo) using DFI technique. These precipitates have also been observed on ageing a directionally solidified eutectic Ni–Al–Mo alloy [27] and the orientation relationship between this precipitate and the matrix was confirmed to be the Nishiyama–Wassermann relationship [18], where $(1\,1\,0)_\alpha \| (0\,0\,1)_\gamma$, $[1\,1\,2]_\alpha \| [1\,1\,0]_\gamma$. In addition, Fig. 5 shows signs of discontinuous transformation at the boundaries, which was observed as early as after 5 min at 700 °C. Since this transformation was not observed at every boundary, the boundaries where the transformation occurred are believed to be grain boundaries rather than cell boundaries. From the DFI of the $\gamma'(Ni_3Al)$ phase (Fig. 5b) it was noted that the matrix of the discontinuous transformation region was $\gamma'(Ni_3Al)$ showing a clear interface between the transformed and the untransformed regions. Discrete $\gamma'(Ni_3Al)$ precipitates within the cells were also observed and the size and shape of this fine precipitate was difficult to determine but seemed to be cuboidal with the unit length being approximately 5 nm. It also shows that the α(Mo) precipitates as indicated by the arrows in Fig. 5a and b form at the transformation boundaries and are left behind as the interface advances into the cells. Higher-magnification micrographs of the transformed grain boundary area in Fig. 5c and d shows the BFI and DFI of α(Mo) phase in the discontinuously transformed region, respectively. The shape of the α(Mo) phase in the transformed region seems to be an irregular disc, whose thickness is approximately equal to the thickness of the α(Mo) precipitates at the cell boundaries (about 15 nm). An attempt to determine the possible orientation relationship between the disc-shaped α(Mo) and the matrix was unsuccessful.

On ageing for 60 min at 700 °C, more plate-like α(Mo) precipitates nucleate and grow in the cells as shown in Fig. 6 and the discontinuous transformation develops further. The discontinuous transformation has an additional driving force from the strain energy associated with the semi-coherent plate-like α(Mo) precipitates within the modulated γ/γ' matrix. As the interface of the transformed region advances into the cells the strain energy associated with the plate-like α(Mo) precipitates is relieved by forming a large disc-shaped α(Mo) phase, resulting in a decrease in total free energy of the system. The modulation wavelength calculated from the inset SADP ($\lambda = 8.0$ nm) is in reasonable agreement with that measured from the BFI (Fig. 6). The inset SADP shows ⟨1 0 0⟩ streaking and this is believed to be due to the discrete $\gamma'(Ni_3Al)$ precipitates as discussed before. However, the contribution of the plate-like α(Mo) precipitate to ⟨1 0 0⟩ streaking must be considered at this stage. Since one of the variants of α(Mo) precipitates lying normal to the thin foil specimen (see Fig. 8c below) has a diffracted spot parallel to $(1\,0\,0)_\gamma$, these plate-like α(Mo) precipitates can also give rise to streaking in $\langle 1\,0\,0\rangle_\gamma$ due to the shape. So, the streaking in the inset SADP in Fig. 6 has two different origins, one from cuboidal $\gamma'(Ni_3Al)$ precipitates from the spinodal ordering and the other from plate-like α(Mo) precipitates from the continuous precipitation. Considering the expected

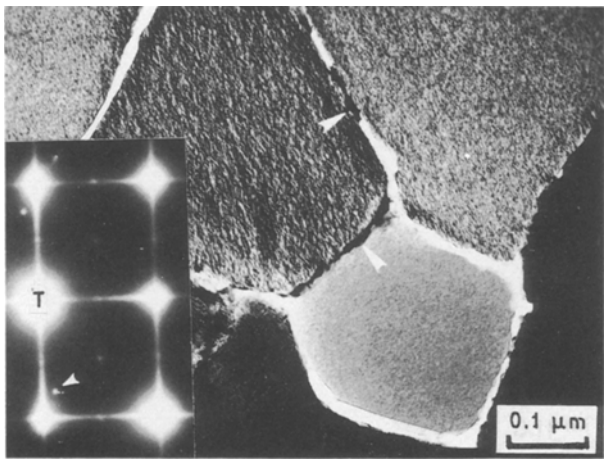

Figure 4 TEM micrographs of ribbon after ageing for 30 min at 650 °C. [0 0 1] zone for the inset diffraction pattern.

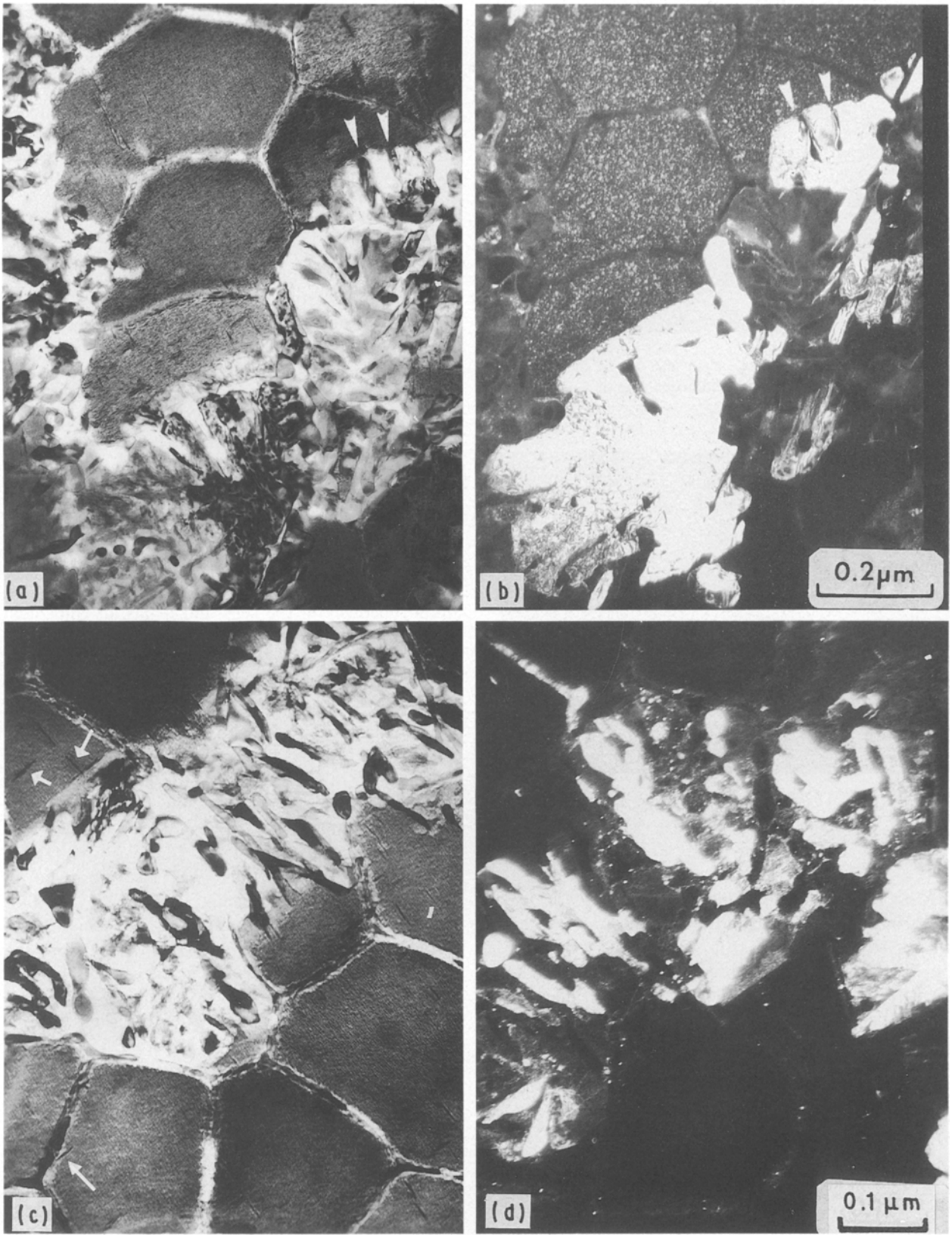

Figure 5 TEM micrographs of ribbon after ageing for 45 min at 700 °C: (a) BF, (b) DF using Ni_3Al superlattice spot, (c) BF of discontinuous transformed grain boundary region, (d) DF using an α(Mo) diffraction spot.

growth of the cuboidal γ′(Ni_3Al) precipitates in the cells and the fact that γ′(Ni_3Al) superlattice spots in the SADP are discrete and not streaked, it is likely that most streaking is due to the shape effect of the thin plate-like α(Mo) precipitates.

After ageing for 120 min at 700 °C, longer and thicker α(Mo) plates were observed within the cells (Fig. 7) and the inset SADP exhibits weak reflections from the metastable Ni_2Mo(Pt_2Mo type) phase and the metastable Ni_3Mo($D0_{22}$), Al_3Ti-type phase as indicated by arrows. The microstructural and diffraction features of 120/700 are very similar to those of 5/800. The ⟨1 0 0⟩ streaking from the fundamental reflections is reduced in length and in intensity as the

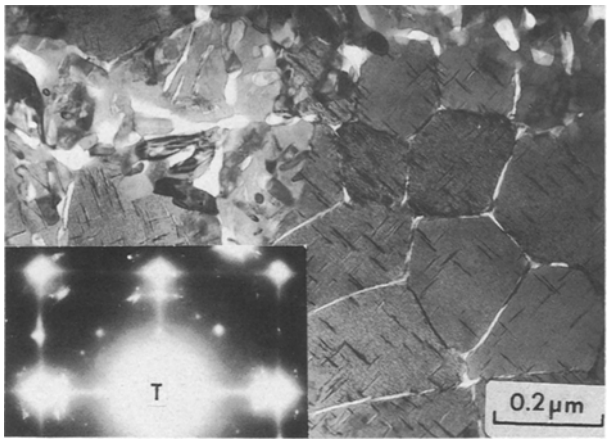

Figure 6 TEM micrograph of ribbon after ageing for 60 min at 700 °C. [0 0 1] zone for the inset diffraction pattern.

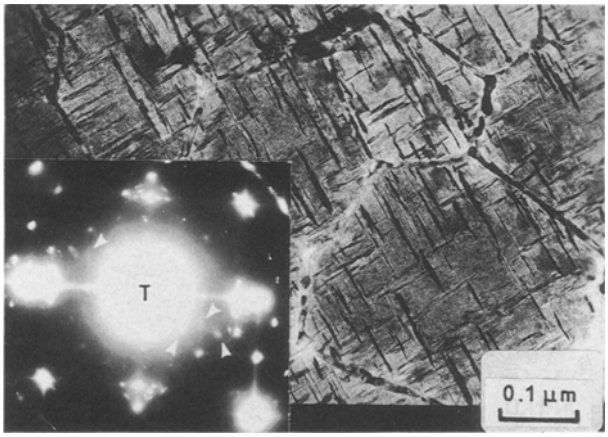

Figure 7 TEM micrograph of ribbon after ageing for 120 min at 700 °C. [0 0 1] zone for the inset diffraction pattern.

α(Mo) plates become thicker. The $Ni_3Mo(D0_{22})$ spots in the inset SADP are elongated in ⟨1 0 0⟩ and weak streaks in ⟨1 0 0⟩ from the elongated $Ni_3Mo(D0_{22})$ spots are present, suggesting that the $Ni_3Mo(D0_{22})$ domains are elongated. The reflections from the metastable Ni_2Mo and $Ni_3Mo(D0_{22})$ phases could not be observed on the microscope screen because of their weak intensities, and long exposures (2–3 min) with an overfocused condenser lens were used to photographically record these spots. DFI of these metastable phases was attempted without success. The plate-like α(Mo) precipitates are of the order of 5–10 nm in thickness. Also at this stage, the α(Mo) plates seem to have coalesced.

After ageing for 300 min at 700 °C, the length of the α(Mo) precipitates in the cell did not seem to increase much, but the α(Mo) phase at the cell boundaries seems to thicken and was measured to be of the order of 15 nm. In comparison the thickness of the α(Mo) at the cell boundaries of 120/700 was of the order of 10 nm as shown in Fig. 7. Fig. 8 shows three orientation variants of the α(Mo) precipitates. Fig. 8a is a BFI and Fig. 8b is a DFI of the α(Mo) plates using the spot indicated by an arrow, showing the various size distributions lying parallel to the surface of the thin foil specimen. Fig. 8c was taken using two spots encircled in the inset SADP in Fig. 8a, showing the α(Mo) plates lying normal to the specimen and the α(Mo) precipitates at the cell boundaries. Fig. 8d shows another variant of the α(Mo) precipitates and it is interesting to note that the α(Mo) plates seem to have coalesced. However, further investigation is needed to identify the growth mechanism more clearly. No work related to the growth mechanism of the plate-like α(Mo) has been reported.

In the SADP of 600/700 (Fig. 9a) the streaks in ⟨1 0 0⟩ were much reduced in intensity and the spots from both metastable phases were still observed. The metastable $Ni_2Mo(Pt_2Mo$ type) spots are indicated by an arrow and $Ni_3Mo(D0_{22})$ spots are indicated by a square in Fig. 9a. These metastable phases were also observed to form during ordering in Ni–Mo alloys [21, 28] and have been discussed extensively by Thomas and co-workers [20, 22]. These Ni_2Mo spots seem to spread into arcs in [4 2 0] directions as previously reported [20, 22, 27]. The spreading of the $\{\frac{2}{3}\,\frac{2}{3}\,0\}$ spots into arcs is mainly due to the shape of this phase [20, 22]. On the other hand the $Ni_3Mo(D0_{22})$ spots were more spherical, compared with those of 120/700 in Fig. 7. The DFI of the Ni_2Mo phase is shown in Fig. 9c. The Ni_2Mo phase nucleates homogeneously in the cells and it has an ellipsoidal shape in the range of 1 to 10 nm in thickness. Also, the sharp appearance, rather than continuous transfer, of the intensity maxima at the Ni_2Mo positions in Fig. 9a as well as in Fig. 7 indicates that the formation of the small, ordered Ni_2Mo precipitates occurs by means of a classical homogeneous nucleation mechanism rather than by spinodal ordering as observed in other Ni–Mo-based ternary alloys [6]. The weak streaking of the $Ni_3Mo(D0_{22})$ spot in ⟨1 0 0⟩ was still present. The streaking of the $\{1\frac{1}{2}0\}$ $Ni_3Mo(D0_{22})$ spots in ⟨1 0 0⟩ directions was also observed in Ni_3(Al, Mo) alloys on ageing at 600 °C [6]. In that case the results were interpreted as formation of $Ni_3Mo(D0_{22})$ phase by spinodal ordering from the short-range ordered matrix as in the case of Ni_3(Mo, X) [6]. This interpretation, however, cannot be applied to this work because the $\{1\frac{1}{2}0\}$ spot in this work is due to the already formed $Ni_3Mo(D0_{22})$ metastable phase, not the short- range ordered matrix. Hence the streaks in ⟨1 0 0⟩ of the $Ni_3Mo(D0_{22})$ spots in this work are likely to be due to the precipitate shape. Dark-field imaging of a superlattice spot as indicated by an arrow in Fig. 9b shows a coarsened cuboidal γ′(Ni_3Al) phase in Fig. 9d. Examination of micrographs of 600/700 reveals that the cells still consist of γ(Ni) + γ′(Ni_3Al) + α(Mo) and the metastable phases of $Ni_3Mo(D0_{22})$ and ellipsoidal Ni_2Mo, and the discontinuous transformation products are γ′(Ni_3Al) and α(Mo) (Figs 10 and 11).

The SADP after 6000 min at 700 °C is similar to that of specimen 300/800 in Fig. 10 and streaking from the fundamental reflections and the metastable Ni_2Mo spots is no longer present. However, the $Ni_3Mo(D0_{22})$ spots are still present. Another phase (Fig. 11a) was observed in the discontinuously transformed region and this phase was identified as equilibrium, orthorhombic, Ni_3Mo phase by indexing the

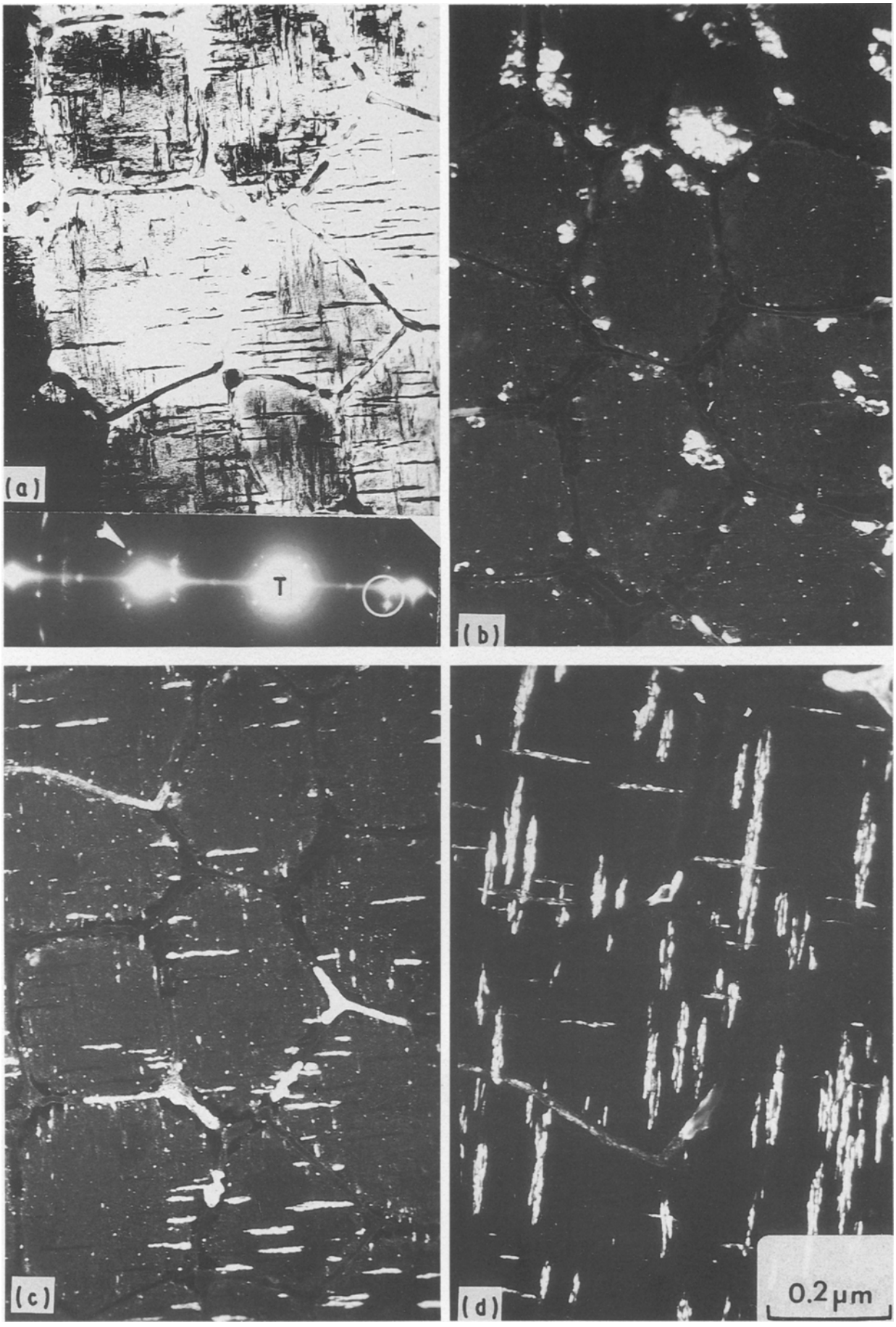

Figure 8 TEM micrographs of ribbon after ageing for 300 min at 700 °C. (a) BF; (b) DF of α(Mo) using a spot indicated by the arrow in the inset SADP in (a); (c) DF of α(Mo) using a spot enclosed in the inset SADP in (a); (d) DF of α(Mo), showing coalescence α(Mo) precipitates.

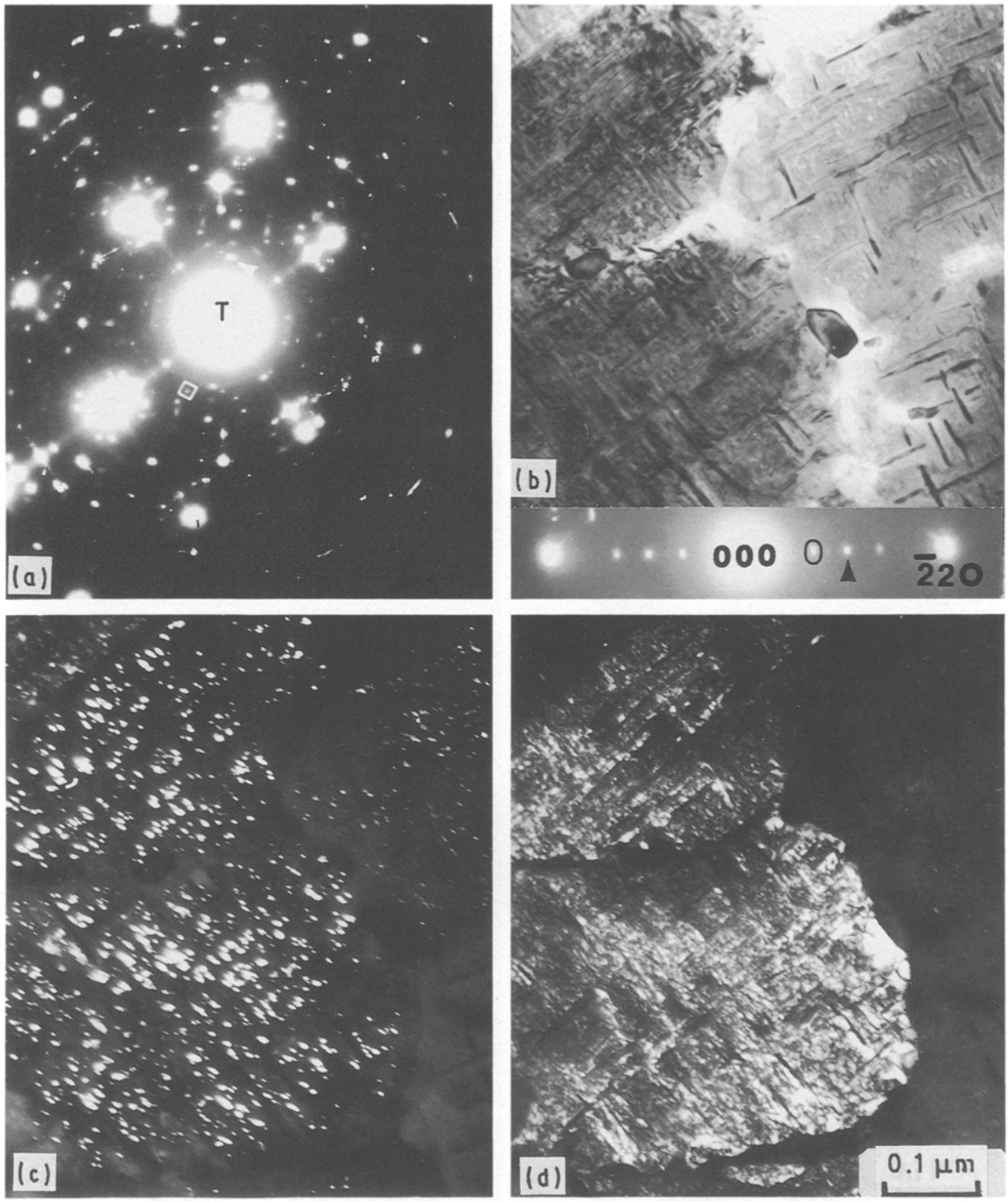

Figure 9 TEM micrographs of ribbon after ageing for 600 min at 700 °C. (a) SADP [0 0 1] zone; (b) BF with inset [0 0 1] SADP; (c) DF of Ni_2Mo using a spot enclosed in the inset SADP in (b); (d) DF of Ni_3Al using a spot indicated by an arrow in the inset SADP in (b).

SADP in Fig. 11b, as shown in Fig. 11d. The orientation relationship between the orthorhombic Ni_3Mo precipitate and the matrix was identified as

$$(1\,0\,0)_p \| (0\,1\,1)_m, [0\,1\,0]_p \| [1\,1\,1]_m$$

confirming the reported orientation relationship between these two phases [21]. Fig. 11c shows the DFI of the orthorhombic Ni_3Mo from the spot encircled in Fig. 11b. The SADP also shows sharp streaking in the $[1\,1\,1]_\gamma \| [0\,1\,0]_p$ direction, which is normal to the thin dimension of the stacking faults in the orthorhombic Ni_3Mo phase. This orthorhombic Ni_3Mo phase was observed previously in Ni–Al–X alloys [29–31]. This phase formed as a product of a cellular precipitation reaction, in which $\gamma(Ni) + \gamma'(Ni_3Al)$ + metastable Ni_xMo transform discontinuously into $\gamma'(Ni_3Al)$ + orthorhombic Ni_3Mo [29].

While the Ni_2Mo spots disappeared completely in specimen 60/800 the $Ni_3Mo(D0_{22})$ spots were still present. Interestingly, spots at $\{\frac{2}{3}\frac{2}{3}0\}$ which apparently represent the metastable Ni_2Mo phase reappeared in 1200/800 (Fig. 12a). Since it is not

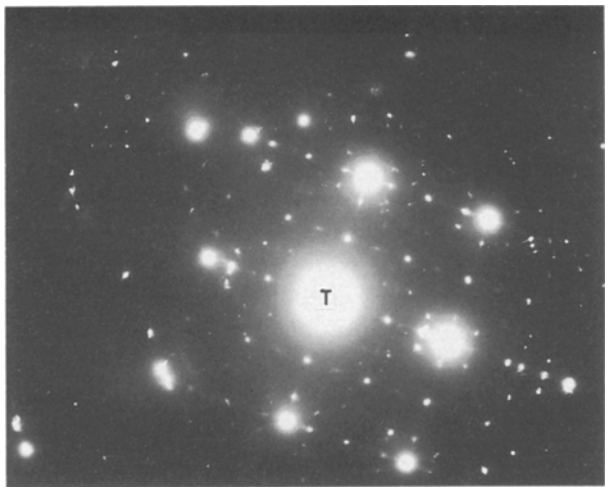

Figure 10 SADP with [001] zone of ribbon after ageing for 300 min at 800 °C.

possible thermodynamically to form this phase again after it has dissolved, extreme care was paid to index the SADP (Fig. 10), especially double diffraction spots originating from different sources which were identified as shown in Fig. 12b. One source of these double diffraction spots is from the fundamental spots (designated α_γ-Mo) and the other double diffraction spots are from the α(Mo) spots (designated α_α-Mo). It was found that the α_α-Mo spots were located at or very close to the spots from the metastable Ni_2Mo phase, $\{\frac{2}{3}\frac{2}{3}0\}$ spots, in Fig. 12a. These are α_α-Mo, not the spots from the Ni_2Mo phase. Diffraction spots corresponding to Ni_4Mo are also close to the $(\frac{2}{3}\frac{2}{3}0)$ position. This suggests that the $Ni_4Mo(D1_a)$ reported earlier [25] on the basis of diffraction spots at the $(\frac{2}{3}\frac{2}{3}0)$ position was misinterpreted. The orthorhombic Ni_3Mo phase was observed on ageing at 800 °C as early as after 300 min at 800 °C and, on long-time ageing to 6000 min at 800 °C, the SADP was similar to the one after 1200 min at 800 °C.

3.1. Isothermal transformation curves

Based on the structural development on ageing of this alloy determined in this and previous work [18, 25], schematic isothermal transformation curves for the phases present, including the metastable phases, were drawn (Fig. 13). Phase transformation sequences on ageing at 800 and 700 °C up to 100 h can be summarized as follows:

$$\gamma(Ni) + \text{short-range order}$$
$$\downarrow$$
$$\gamma(Ni) + \gamma'(Ni_3Al)$$
$$\downarrow$$
$$\gamma(Ni) + \gamma'(Ni_3Al) + \alpha(Mo)_b$$
$$\downarrow$$
$$\gamma(Ni) + \gamma'(Ni_3Al) + \alpha(Mo)_b + \alpha(Mo)_p$$
$$\downarrow$$
$$\gamma(Ni) + \gamma'(Ni_3Al) + \alpha(Mo)_b + \alpha(Mo)_p + Ni_2Mo + Ni_3Mo(D0_{22})$$
$$\downarrow$$
$$\gamma(Ni) + \gamma'(Ni_3Al) + \alpha(Mo)_b + \alpha(Mo)_p + Ni_3Mo(D0_{22}) + Ni_3Mo$$

where $\alpha(Mo)_b$ represents the α(Mo) precipitates at the boundaries and $\alpha(Mo)_p$ represents the plate-like α(Mo) precipitates within the cells. The supersaturated γ(Ni) matrix decomposes by spinodal ordering in the very early stage of ageing, resulting in a modulated γ/γ′ matrix. α(Mo) phase then forms both by heterogeneous nucleation at the cell boundaries and by homogeneous nucleation within the cells. The α(Mo) at the cell boundaries probably forms first and the plate-like α(Mo) precipitates homogeneously from the γ/γ′ matrix in the cells after a short incubation period.

The observation of α(Mo) at cell boundaries as well as homogeneous precipitation of the α(Mo) within the cells can be explained as follows. On ageing, Mo atoms will diffuse fast along the cell boundaries to form the precipitates in the boundaries first. While the spinodal ordering occurs within the cells, the γ/γ′ matrix is still in a metastable state since it is still supersaturated with Mo. Assuming that all the Mo is trapped within the γ/γ′ matrix without α(Mo) precipitation, the matrix is supersaturated with Mo by about 4 to 14 at % because the maximum equilibrium Mo contents in γ(Ni) and γ′(Ni_3Al) phases at 800 °C are about 15 and 5 at % Mo, respectively [32]. This is a reasonable assumption since Mo is expected to be very slow to diffuse out of the γ(Ni) and γ′(Ni_3Al) phases. Therefore, on further ageing the γ(Ni) and γ′(Ni_3Al) phases will try to attain equilibrium Mo contents by diffusion of Mo to the interface between the γ(Ni) and γ′(Ni_3Al) phases. This results in precipitation of semi-coherent α(Mo) at these interfaces. This heterogeneous nucleation and growth of the plate-like α(Mo) precipitates continues until the supersaturation of Mo has been reduced to an equilibrium level and coarsening begins. Coarsening of this phase is observed after 300 min at 700 °C as shown in Fig. 8d. The metastable phases Ni_2Mo and $Ni_3Mo(D0_{22})$ form homogeneously in the γ/γ′ matrix while the nucleation of plate-like α(Mo) precipitates stops as shown by the electrical resistivity experiments discussed in Part II [17]. It is not clear which one forms first, but the ellipsoidal Ni_2Mo phase disappears before the $Ni_3Mo(D0_{22})$ phase does. Even though the morphology of the $Ni_3Mo(D0_{22})$ phase was not definitely established in this work, it is suspected that it has a lath shape, based on the streaking in ⟨100⟩ of the spots in the SADP in Fig. 10. It was reported that $Ni_3Mo(D0_{22})$ phase formed as laths on the orthogonal {100} faces of γ′(Ni_3Al) particles in an Ni–Al–Mo–Ta alloy [10] and Inconel 718 [33]. Al is reported to stabilize the $Ni_3Mo(D0_{22})$ phase [5, 6] by decreasing the V_2/V_1 ratio (ratio of second and first nearest-neighbour interaction parameters) in the theory developed by Sanchez and de Fontaine [34]. Therefore the stability of $Ni_3Mo(D0_{22})$ phase up to 1000 °C is believed to be due to the large amount of Al in this alloy. A discontinuous transformation was observed at the grain boundaries as early as in specimen 5/700. In the early stage of ageing, it involves

$$\gamma(Ni) + \gamma'(Ni_3Al) + \alpha(Mo) \rightarrow \gamma'(Ni_3Al) + \alpha(Mo)$$

which can be defined as a discontinuous coarsening. However, a more complex type of discontinuous transformation was observed in the later stage of

ageing involving

$$\gamma(\mathrm{Ni}) + \gamma'(\mathrm{Ni_3Al}) + \alpha(\mathrm{Mo}) + \mathrm{Ni_3Mo}(\mathrm{D0_{22}}) + \mathrm{Ni_2Mo} \rightarrow \gamma'(\mathrm{Ni_3Al}) + \alpha(\mathrm{Mo}) + \text{equilibrium } \mathrm{Ni_3Mo}$$

Equilibrium orthorhombic Ni_3Mo phase was also observed after ageing at 800 and 700 °C but not at 650 °C. Even though slow kinetics at 650 °C might be a reason for not observing Ni_3Mo phase, it could also be an indication that the upper solvus of this phase is between 650 and 700 °C. Ni_3Mo has been observed as a product of a cellular precipitation reaction occurring at grain boundaries in Ni–Al–Mo [30] and in Ni–Al–Mo–Ta [29]. Hence the Ni_3Mo phase in this alloy is expected to form as a product of the discontinuous transformation. The orthorhombic Ni_3Mo phase has been reported to cause a substantial loss in ductility [29]. More importantly, the embrittling δ(NiMo) phase was not found at temperatures at or lower than 800 °C up to 100 h. Whether it is really the effect of the V addition in reducing the δ(NiMo) phase region or it is simply a matter of kinetics is not clear and requires further work.

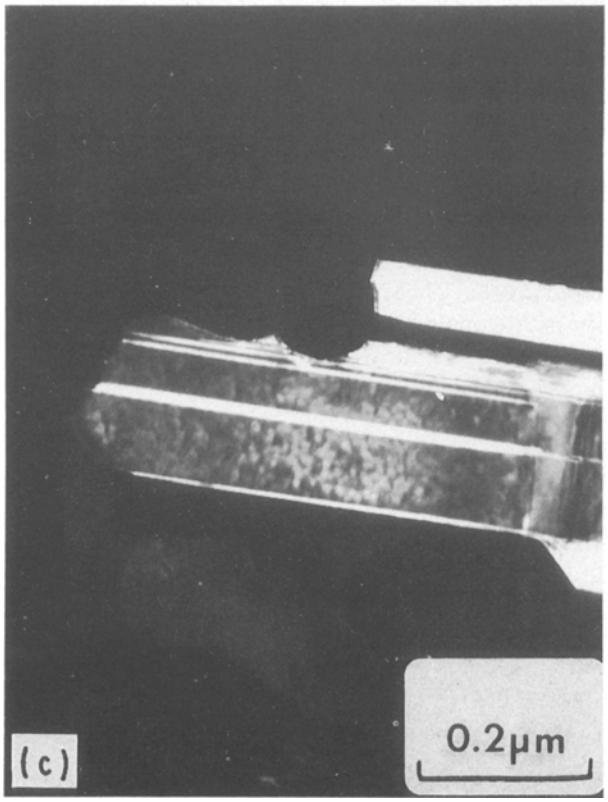

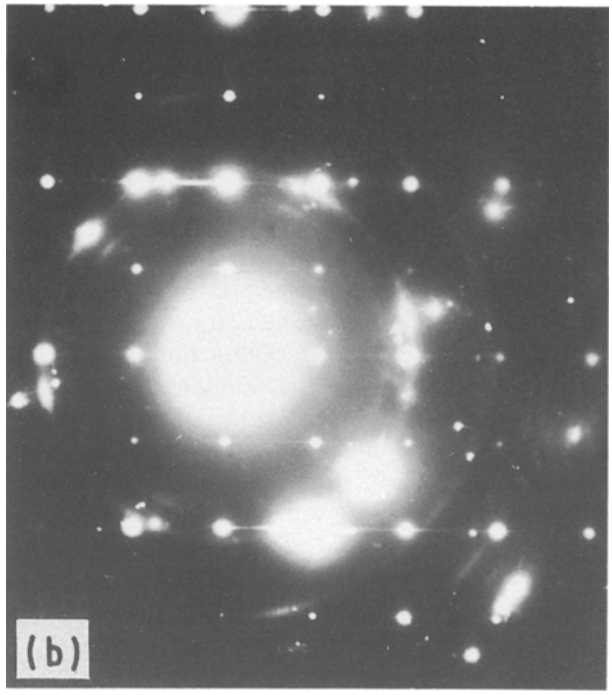

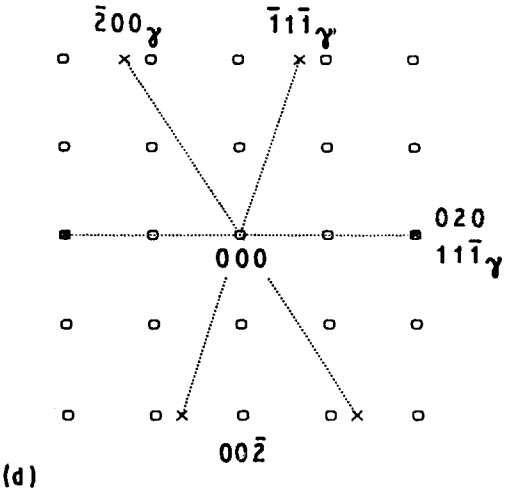

Figure 11 Equilibrium, orthorhombic Ni_3Mo phase observed after ageing for 6000 min at 700 °C. (a) BF; (b) SADP with $g = [001]_{Ni_3Mo} = [011]_{f.c.c.}$; (c) DF of Ni_3Mo; (d) indexed SADP: (○) Ni_3Mo, (×) matrix.

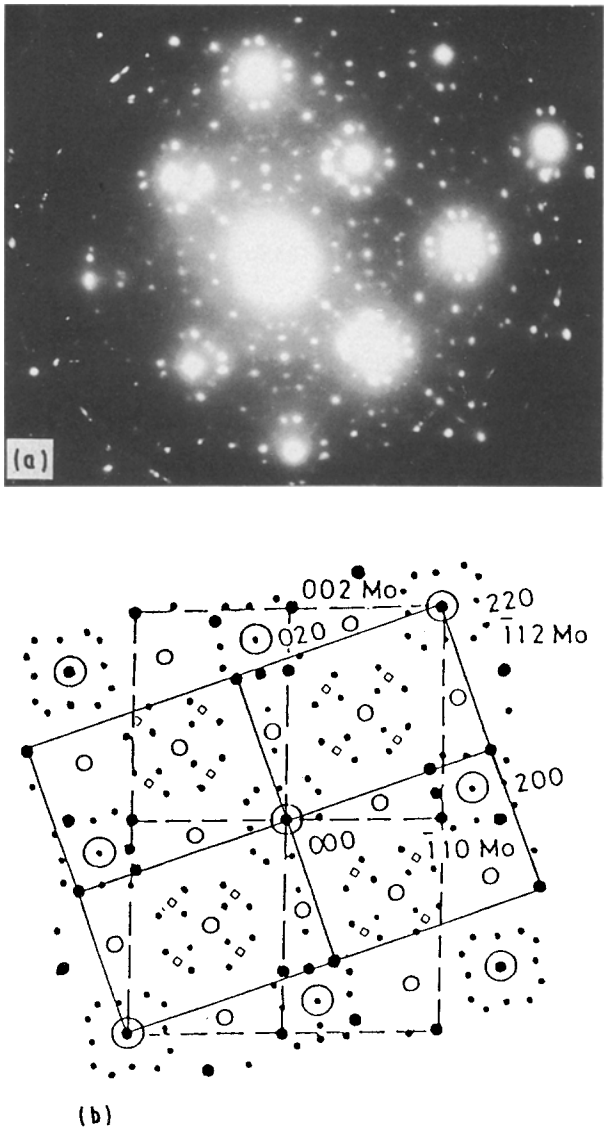

Figure 12 Ribbon after ageing for 1200 minutes at 800 °C. (a) SADP with [0 0 1] zone; (b) a schematic indexed SADP with [0 0 1] zone, showing the double diffracted spots from two origins, α_γ(Mo) = double-diffracted α(Mo) spots diffracted from fundamental f.c.c. diffracted spots, α_α = double-diffracted α(Mo) spots diffracted from diffracted α(Mo) spots. (○) Fundamental f.c.c. spots, (○) superlattice Ni_3Al spots, (●)α(Mo) spots, (●) α_α double-diffraction spots, (◇) α_γ double-diffraction spots.

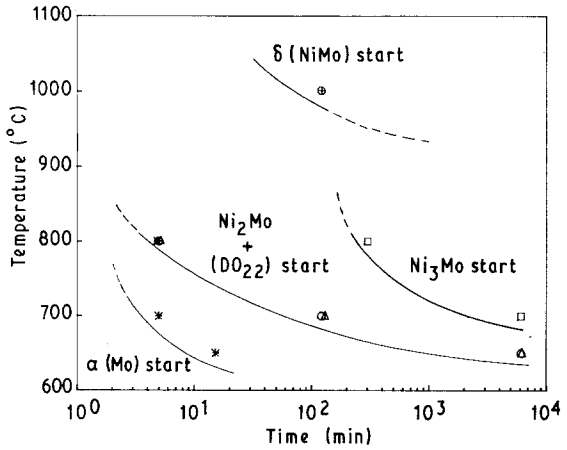

Figure 13 Partial isothermal transformation curves for the phases observed in the alloy. (○) $Ni_3Mo(D0_{22})$, (*) α(Mo), (△) Ni_2Mo, (□) equilibrium Ni_3Mo, (+) δ(NiMo).

4. Summary and conclusions

The phase transformation sequences during ageing of rapidly solidified Ni–Al–Mo–V–Re in the range from 800 to 650 °C for up to 100 h have been identified. The transformation behaviour of this alloy was independent of the ageing temperature over this range, simply showing enhanced kinetics with increasing temperature. Due to the large amount of Al in the alloy the metastable $Ni_3Mo(D0_{22})$ phase was more stable than the metastable Ni_2Mo phase. The addition of a small amount of V to the eutectic alloy composition resulted in the δ(NiMo) phase not being observed after ageing up to 100 h at temperatures at or below 800 °C. An isothermal transformation diagram summarizing the transformation events has been deduced.

A discontinuous transformation was observed at the grain boundaries. While the reaction was determined to be a discontinuous coarsening reaction in the early stage of ageing, it became a more complex discontinuous transformation at the later stage, involving metastable phases and the equilibrium orthorhombic Ni_3Mo.

The results of this study are correlated with the physical and mechanical properties of the material in the following paper, Part II [17].

Acknowledgements

This paper is based on work by S.Y.L. in partial fulfillment of the requirements for the PhD degree at Illinois Institute of Technology. The authors wish to thank the NASA Lewis Research Center for material preparation and also thank Dr Nestor Zaluzec and Mr Russ Cook at Argonne National Laboratory for provision of TEM facilities. One of the authors (S.Y.L) gratefully acknowledges financial support provided by the Department of Metallurgical and Materials Engineering at Illinois Institute of Technology.

References

1. W. SOFFA and D. LAUGHLIN, in Proceedings of International Conference on Solid–Solid Phase Transformation, Camegie-Mellon, Pittsburgh, Pennsylvania, USA, August 10–14, 1981, edited by H. Aaronson, D. Laughlin, R. Sekerka and C. Wayman (AIME, Warrendale, 1982) p. 159.
2. G. Van TENDELOO, J. Van LANDUYT, P. DELAVIGNETTE and S. AMELINCKX, *Phys. Status Solidi (a)* **25** (1974) 299.
3. G. Van TENDELOO, R. de RIDDER and S. AMELINCKX, *ibid.* **27** (1975) 247.
4. K. VASUDEVAN and E. STANSBURY, in Proceedings of Conference on Materials Problem Solving with the Transmission Electron Microscope, Boston 1985 MRS Proceedings Vol. **62** (MRS, Pittsburgh, 1986) p. 337.
5. M. YAMAMOTO, F. SHOHNO and S. NENNO, *Trans. J. Inst. Met.* **19** (1978) 475.
6. P. MARTIN and J. WILLIAMS, *Acta Metall* **32** (1984) 1681.
7. E. VLASOVA, Y. TYAPKIN and V. PLAKHTII, *Sov. Phys. Dokl.* **10** (1974) 32.
8. P. MARTIN, H. LIPSITT and J. WILLIAMS, in Proceedings of Conference on Rapid Solidification Processing Principles and Technologies, Camegie-Mellon, Pittsburgh, Pennsylvania, USA, August 10–14, 1981, edited by R. Mehrabian, B. Kear and M. Cohen (Claitor's, Baton Rouge, 1978) p. 123.
9. P. MARTIN and J. WILLIAMS, in Proceedings of International Conference on Solid–Solid Phase Transformation,

Reston, Virginia, USA, November 13–16, 1977, edited by H. Aaronson, D. Laughlin, R. Sekerka, and C. Wayman (AIME, Warrendale, 1982) p. 757.
10. J. WILLIAMS and P. MARTIN, *Met. Trans. A* **16A** (1985) 1983.
11. S. LEE, PhD thesis, Illinois Institute of Technology (1988).
12. P. CLAPP and S. MOSS, *Phys. Rev.* **142** (1966) 418.
13. *Idem, ibid.* **171** (1968) 754.
14. S. MOSS and P. CLAPP, *ibid.* **171** (1968) 764.
15. D. de FONTAINE, *Acta Metall.* **23** (1975) 553.
16. *Idem, Solid State Phys.* **34** (1979) 73.
17. S. LEE and P. NASH, *J. Mater. Sci.* **28** (1993) 1957.
18. S. LEE, P. NASH and S. BRADLEY, *ibid.* **25** (1990) 1219.
19. S. DAS, P. OKAMOTO, P. FISHER and G. THOMAS, *Acta Metall.* **21** (1973) 913.
20. S. DAS and G. THOMAS, *Phys. Status Solidi (a)* **21** (1974) 177.
21. M. YAMAMOTO, S. NENNO, T. SABURI and Y. MIZUTANI, *Trans. J. Inst. Met.* **11** (1970) 120.
22. P. OKAMOTO and G. THOMAS, *Acta Metall.* **19** (1971) 825.
23. L. NESBITT and D. LAUGHLIN, *ibid.* **26** (1978) 815.
24. V. DANIEL and H. LIPSON, *Proc. R. Soc.* **A181** (1943) 368.
25. P. NASH and T. GLASGOW, *Acta Metall.* **35** (1987) 2627.
26. J. EDINGTON, "Practical Electron Microscopy in Materials Science" (Van Nostrand Reinhold, New York, 1976) p. 88.
27. M. NEMOTO, T. HONDA, Y. NAKAGAWA, Y. SAIGA and H. SUTO, *Trans. J. Inst. Met.* **21** (1980) 505.
28. T. SABURI, K. KOMATSU, M. YAMAMOTO and S. NENNO, *Trans. AIME.* **245** (1969) 2348.
29. D. SNOW, E. BRENIAN and B. KEAR, in "Superalloy 1980", edited by J. Tien, S. Woldek, H. Morrow III, M. Gell and G. Maurer (ASM, Materials Park, Ohio, 1980) p. 189.
30. M. KAUFMAN, J. EADES, H. LORETTO and H. FRASER, *Met. Trans. A* **14A** (1983) 1561.
31. K. VASUDEVAN and E. STANSBURY, *Scripta Metall.* **19** (1985) 1101.
32. S. LEE, K. J. LEE and P. NASH, in "Phase Diagrams of Binary Nickel Alloys" Ed. P. Nash (ASM International, Materials Park, Ohio, 1991).
33. R. COZAR and A. PINEAN, *Met. Trans. A* **4A** (1973) 47.
34. J. SANCHEZ and D. de FONTAINE, *Phys. Rev. B* **25** (1982) 1759.

Received 8 May
and accepted 11 June 1992